Star Formation News Letter No. 370, #41-54：工藤哲洋

2

41. **Sandwiched planet formation: restricting the mass of a middle planet**
Matthew Pritchard, Farzana Meru, Sahl Rowther, David Armstrong, Kaleb Randall ★ We conduct gas and dust

42. **Dust Coagulation Reconciles Protoplanetary Disk Observations with the Vertical Shear Instability – Part I: Dust Coagulation and the VSI Dead Zone**
Thomas Pfeil, Til Birnstiel, Hubert Klahr ★ Protoplanetary disks exhibit a vertical gradient in angular momentum,

43. **The Corona Australis complex is accelerating away from the Galactic plane**
L. Posch, N. Miret-Roig, J. Alves, S. Ratzenböck, J. Großschedl, S. Meingast, C. Zucker, A. Burkert ★ We

44. **NEATH II: N_2H^+ as a tracer of imminent star formation in quiescent high-density gas**
F. D. Priestley, P. C. Clark, S. C. O. Glover, S. E. Ragan, O. Fehér, L. R. Prole, R. S. Klessen ★ Star

45. **Neural network-based emulation of interstellar medium models**
Pierre Palud, Lucas Einig, Franck Le Petit, Emeric Bron, Pierre Chainais, Jocelyn Chanussot, Jérôme Pety, Pierre-Antoine Thouvenin, David Languignon, Ivana Bešlić, Miriam G. Santa-Maria, Jan H. Orkisz, Léontine E. Ségal, Antoine Zakardjian, Sébastien Bardeau, Maryvonne Gerin, Javier R. Goicoechea, Pierre Gratier, Viviana V. Guzman, Annie Hughes, François Levrier, Harvey S. Liszt, Jacques Le Bourlot, Antoine Roueff, Albrecht Sievers ★ The interpretation of observations of atomic and molecular tracers in the galactic and extragalactic

46. **Wind erosion and transport on planetesimals**
A. C. Quillen, Stephen Luniewski, Adam E. Rubinstein, Jeremy Couturier, Rachel Glade ★ We consider the

3

47. **Protoplanetary and debris disks in the η Chamaeleontis Association: A sub-millimeter survey obtained with APEX/LABOCA**
V. Roccatagliata, A. Sicilia-Aguilar, M. Kim, J. Campbell-White, M. Fang, S. J. Murphy, S. Wolf, W. A. Lawson, Th. Henning, J. Bouwman ★ Nearby associations are ideal regions to study coeval samples of protoplanetary and

1

48. **A High-Mass Young Star-forming Core Escaping from Its Parental Filament**
Zhiyuan Ren, Xi Chen, Tie Liu, Emma Mannfors, Leonardo Bronfman, Fengwei Xu, Siyi Feng, Hongli Liu, Fanyi Meng, Amelia. M. Stutz, Shanghuo Li, Chang Won Lee, Ke Wang, Jianwen Zhou, Di Li, Chen Wang, Chakali Eswaraiah, Anandmayee Tej, Long-Fei Chen, Hui Shi ★ We studied the unique kinematic properties in

49. **Modelling Deuterated Isotopologues of Methanol toward the Pre-Stellar Core L1544**
W. Riedel, O. Sipilä, E. Redaelli, P. Caselli, A. I. Vasyunin, F. Dulieu, N. Watanabe ★ Aims. We aim to improve a

50. **Protoplanetary disks in K_s-band total intensity and polarized light**
Bin B. Ren, Myriam Benisty, Christian Ginski, Ryo Tazaki, Nicole L. Wallack, Julien Milli, Antonio Garufi, Jaehan Bae, Stefano Facchini, François Ménard, Paola Pinilla, C. Swastik, Richard Teague, Zahed Wahhaj

51. **XUE. Molecular inventory in the inner region of an extremely irradiated Protoplanetary Disk**
María Claudia Ramirez-Tannus, Arjan Bik, Lars Cuijpers, Rens Waters, Christiane Goppl, Thomas Henning, Inga Kamp, Thomas Preibisch, Konstantin V. Getman, Germán Chaparro, Pablo Cuartas-Restrepo, Alex de Koter, Eric D. Feigelson, Sierra L. Grant, Thomas J. Haworth, Sebastián Hernández, Michael A. Kuhn, Giulia Perotti, Matthew S. Povich, Megan Reiter, Veronica Roccatagliata, Elena Sabbi, Benoît Tabone, Andrew J. Winter, Anna F. McLeod, Roy van Boekel, Sierk E. van Terwisga ★ We present the first results of the eXtreme UV

52. **Illuminating evaporating protostellar outflows: ERIS/SPIFFIER reveals the dissociation and ionization of HH 900**
Megan Reiter, Thomas J. Haworth, Carlo F. Manara, Suzanne Ramsay, Pamela D. Klaassen, Dominika Itrich, Anna F. McLeod ★ Protostellar jets and outflows are signposts of active star formation. In H II regions, molecular tracers

53. **Stable accretion in young stars: The cases of EX Lupi and TW Hya**
A. Sicilia-Aguilar, J. Campbell-White, V. Roccatagliata, J. Desira, S. G. Gregory, A. Scholz, M. Fang, F. Cruz-Saenz de Miera, Á. Kóspál, S. Matsumura, P. Ábrahám ★ We examine the long-term spectroscopic and photometric

54. **Formation of misaligned second-generation discs through flyby encounters**
Jeremy L. Smallwood, Rebecca Nealon, Nicolás Cuello, Ruobing Dong, Richard A. Booth ★ Observations reveal

48. **A High-Mass Young Star-forming Core Escaping from Its Parental Filament**

Zhiyuan Ren, Xi Chen, Tie Liu, Emma Mannfors, Leonardo Bronfman, Fengwei Xu, Siyi Feng, Hongli Liu, Fanyi Meng, Amelia. M. Stutz, Shanghuo Li, Chang Won Lee, Ke Wang, Jianwen Zhou, Di Li, Chen Wang, Chakali Eswaraiah, Anandmayee Tej, Long-Fei Chen, Hui Shi

★ We studied the unique kinematic properties in massive filament G352.63-1.07 at 10^3-AU spatial scale with the dense molecular tracers observed with the Atacama Large Millimeter/submillimeter Array (ALMA). We find the central massive core M1 (12 $M_\odot$) being separated from the surrounding filament with a velocity difference of $v - v_{sys} = -2$ km/s and a transverse separation within 3 arcsec. Meanwhile, as shown in multiple dense-gas tracers, M1 has a spatial extension closely aligned with the main filament and is connected to the filament towards its both ends. M1 thus represents a very beginning state for a massive young star-forming core escaping from the parental filament, within a time scale of $\sim$ 4000 years. Based on its kinetic energy (3.5×10^{44} erg), the core escape is unlikely solely due to the original filament motion or magnetic field, but requires more energetic events such as a rapid intense anisotropic collapse. The released energy also seems to noticeably increase the environmental turbulence. This may help the filament to become stabilized again.

- コアがフィラメントから分離しているところを発見した。
- 分離速度　–2 km/s，タイムスケール～4000年。
- 乱流のエネルギーは小さいので，異方性のコア収縮が原因か？

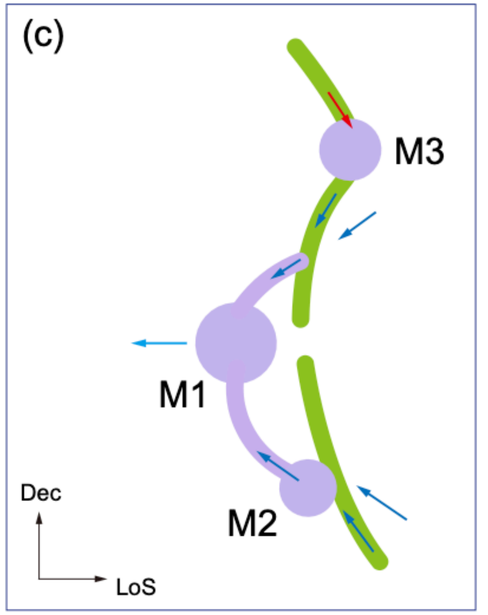

Table 1. The physical properties of the cores.

Parameters	M1	M2	M2b	M3	M4	M5
(Observed)						
$v_{\rm lsr}$ ($H^{13}CO^+$) (km s^{-1})	-2.5	-0.8	-0.6	+0.1	+1.0	+1.3
$T_{\rm ex}$ (HCO^+) (K)	37	22	22	22	22	20
$T_{\rm b}$ ($H^{13}CO^+$) (K)	4.0	3.0	5.0	2.1	3.7	2.6
Δv (km s^{-1})	2.5	2.3	1.8	2.2	1.8	1.7
Radius (arcsec)[a]	5	4	6	5	4	4
(Derived)						
$N_{\rm tot}$ (10^{23} cm^{-2}) [b]	2.6 ± 0.3	2.2 ± 0.2	2.3 ± 0.3	2.4 ± 0.2	2.2 ± 0.2	2.2 ± 0.2
$\sigma_{\rm tot}$ (km s^{-1})	1.1	0.9	0.8	1.0	0.7	0.7
Mass ($M_\odot$)	12 ± 2	6 ± 2	11 ± 2	8 ± 2	7 ± 2	7 ± 2
$m_{\rm crit}$ ($M_\odot$)	15	13	12	12	11	11

a. Average radius deconvolved with the beam size.
b. $N_{\rm tot}$ is derived from $H^{13}CO^+$ intensity using Equation A4. For M4 and M5, th
$H^{13}CO^+$ emissions are noticeably dissipated by the outflows. We assumed them t
have same $N_{\rm tot}$ with M3 based on the fact that these cores also have comparable
mm continuum emissions.

コアはほぼサブクリティカル

フィラメント全体もサブクリティカル

$$\left(\frac{M}{l}\right)_{\rm crit} = \frac{2\sigma_{\rm tot}^2}{G}. \qquad (2)$$

$$(M/l)_{\rm obs} < (M/l)_{\rm crit}$$

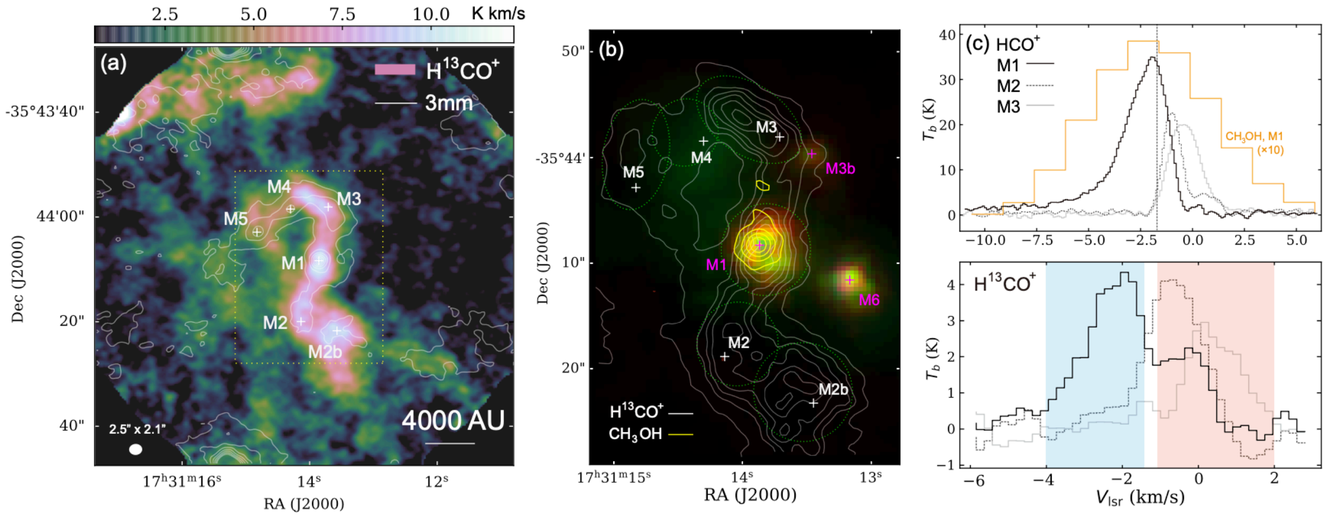

Figure 1. **(a)** The velocity-integrated intensity of the $H^{13}CO^+$ (1-0) line (false-color) and 3 mm continuum. The contour levels are $4\sigma_{\rm rms}$ (1.6 mJy beam^{-1}) to $84\sigma_{\rm rms}$ (peak) in step of $16\sigma_{\rm rms}$. **(b)** The $H^{13}CO^+$ and CH_3OH emission regions around the main filament, overlaid on the IRAC-RGB image (3.6, 4.5, and 8.0 μm bands). The $H^{13}CO^+$ contours are 15% to 90% in 15%-step of the peak intensity (8.5 K km s^{-1}). The CH_3OH contours are 10% to 90% in 20%-step of the peak intensity (18.7 K km s^{-1}). The dashed circles labels the area of each core. **(c)** The spectra at the selected core centers. The blue and red-shaded areas indicate the velocity ranges of the two velocity components, respectively. The vertical dashed line denotes the division between the blue and main-filament components.

PV図

$H^{13}CO^+$

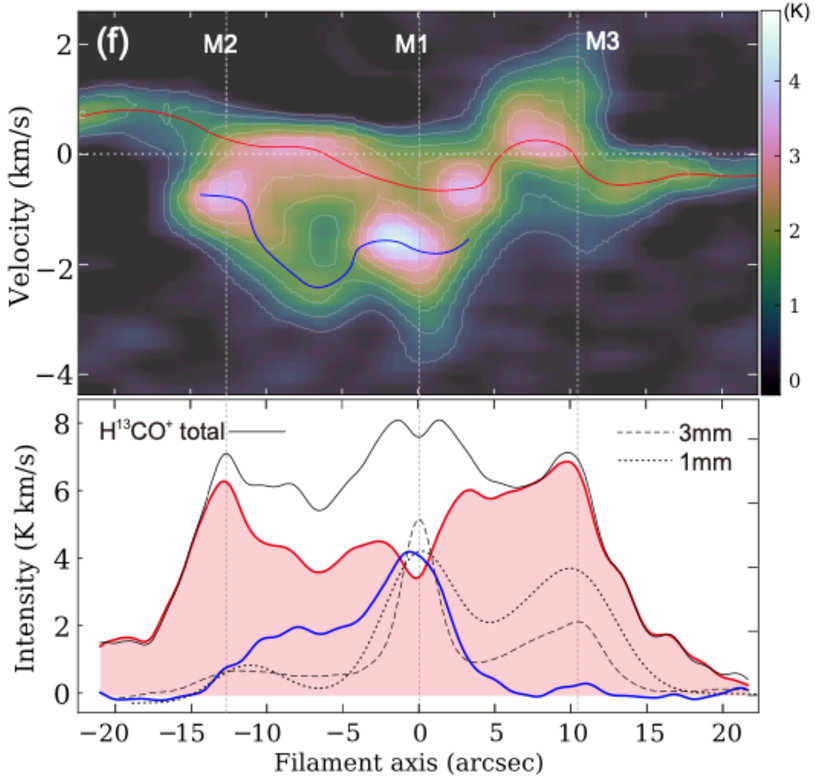

onto the filament. **(b)** PV plot and intensity profile along the major axis of the main filament. The sampling direction is labelled in dashed line in panel (a). The vertical dashed lines denote the projected offset of the three dense cores on the sampling direction. The horizontal dotted line represents the average systemic velocity of the filament.

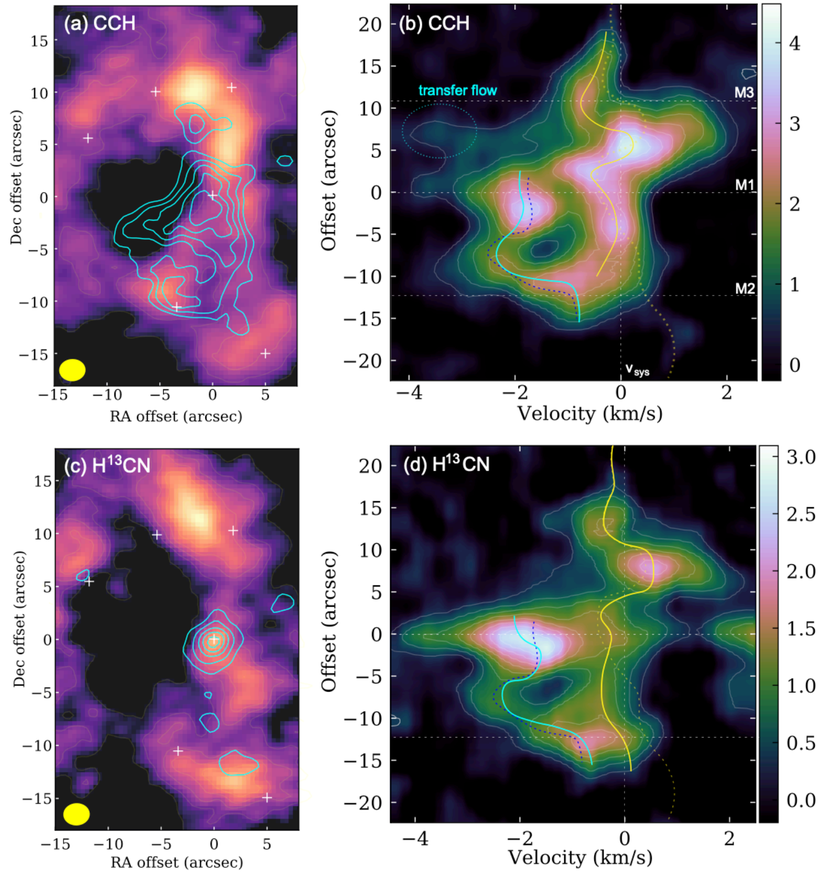

CCH

$H^{13}CN$

Figure 3. Left column: The emission regions of the blue- (contours) and redshifted (false-color) components in CCS and $H^{13}CN$ (1-0) lines. The contour levels are 20% to 90% of the peak intensity. **Right column:** The PV diagrams of the two molecular lines. the $H^{13}CN$ emission at $v_{\rm lsr} = 2$ to 4 km s^{-1} is from anther HFC of $F = 1 - 1$. The HFCs of $H^{13}CN$ are separated for 6-7 km s^{-1} and would not blend with each other. The CCH (1-0) emission shows an additional small blueshift wings around M3, which should correspond to the transfer flow onto the filament (Chen21). This feature is not seen in other lines probably because of their lower optical depths.

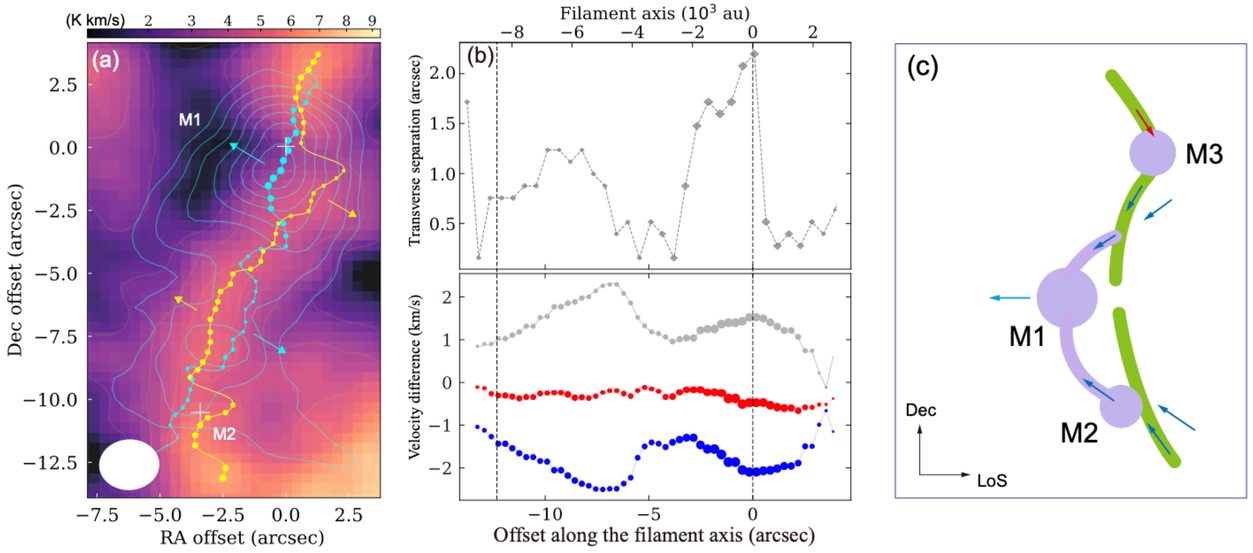

Figure 5. **(a)** The ridge lines of the two velocity components, blue component in blue line and dots, red-center component (main filament) in yellow line and dots. The dot size is proportional to the integrated intensity. The arrows denote the projected moving direction of each component expected on the sky-plane. **(b)** The transverse offset and velocity difference between the ridge lines of the two components along the filament axis. In the lower panel, the blue and red dots represent the peak radial velocity profile of the two components, respectively. The gray dots represent $|v_{\rm blue} - v_{\rm red}|$. **(c)** A schematic view of the gas motion on the filament and cores.

著者が推測しているシナリオ

(i)フィラメントは比較的低い乱流を持ち、コアに分裂。

(ii)フィラメントに沿った流れのため質量が大きく不安定になり、最終的には重力崩壊。

(iii)M1は重力崩壊によって強く圧縮され脱出運動を開始。残りのエネルギーはフィラメントに伝達され乱流を増加。

41. Sandwiched planet formation: restricting the mass of a middle planet

Matthew Pritchard, Farzana Meru, Sahl Rowther, David Armstrong, Kaleb Randall ★ We conduct gas and dust hydrodynamical simulations of protoplanetary discs with one and two embedded planets to determine the impact that a second planet located further out in the disc has on the potential for subsequent planet formation in the region locally exterior to the inner planet. We show how the presence of a second planet has a strong influence on the collection of solid material near the inner planet, particularly when the outer planet is massive enough to generate a maximum in the disc's pressure profile. This effect in general acts to reduce the amount of material that can collect in a pressure bump generated by the inner planet. When viewing the inner pressure bump as a location for potential subsequent planet formation of a third planet, we therefore expect that the mass of such a planet will be smaller than it would be in the case without the outer planet, resulting in a small planet being sandwiched between its neighbours - this is in contrast to the expected trend of increasing planet mass with radial distance from the host star. We show that several planetary systems have been observed that do not show this trend but instead have a smaller planet sandwiched in between two more massive planets. We present the idea that such an architecture could be the result of the subsequent formation of a middle planet after its two neighbours formed at some earlier stage.

- 原始惑星円盤と惑星との相互作用の流体数値シミュレーション
- 二つの大きな惑星ができた場合，その間に小さな惑星ができる可能性を示した。（標準モデルでは，恒星から遠くなると惑星質量が大きくなると予想しているが。）
- 実際にそのような惑星系の観測結果も示す。

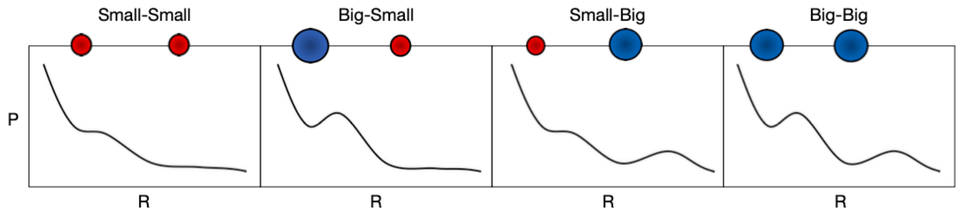

Figure 1. Schematic illustration of disc pressure profiles in the four cases we explore in our main suite of simulations. "Small" and "Big" refer to low and high mass planets, which cause the pressure profile exterior to the planet to form a point of inflection and a pressure maximum, respectively.

- 等温流体＋ダスト＋惑星の数値シミュレーション

$$\Sigma = \Sigma_0 \left(\frac{R}{R_0}\right)^{-1}$$,（面密度）

$$\left(\frac{H}{R}\right) = 0.05 \left(\frac{R}{R_0}\right)^{0.25}$$ （スケールハイト）

$\alpha = 10^{-3}$ （α粘性）

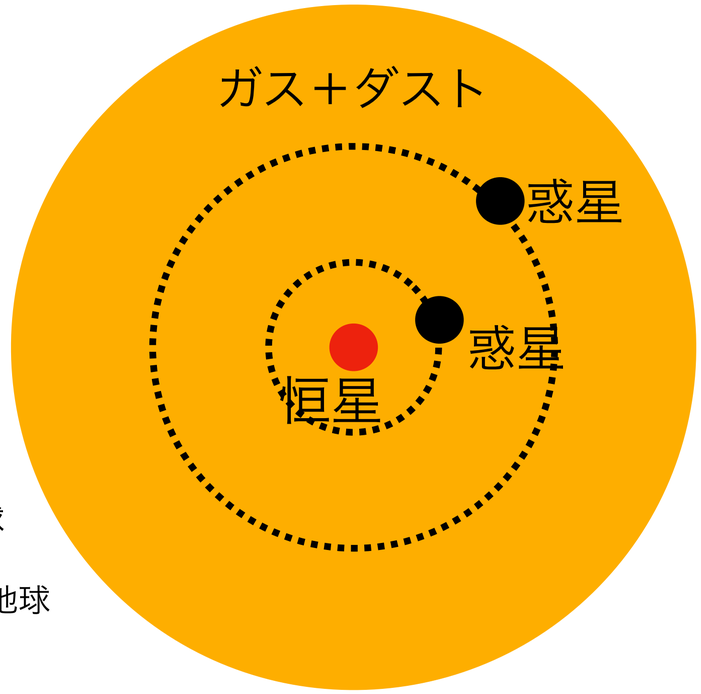

恒星質量＝1M太陽

内側惑星質量＝12 or 20 M地球

外側側惑星質量＝20 or 35 M地球

ダストのストークス数：0.002, 0.02, 0.2

ストークス数Stは次式で定義される

$$St = \frac{\rho_p d^2 U}{18 \eta L}$$

- ρ_p ： 微粒子の密度(kg/m3)
- d ： 微粒子の直径(m)
- U ： 流れの代表速さ(m/s)
- η ： 流体の粘性(kg/m s)
- L ： 流れの代表長さ(m)

流体中を運動する微粒子について、流体への追従性を表す。St <<1 の場合にダストは流体と一緒に動く。

Wikipedia

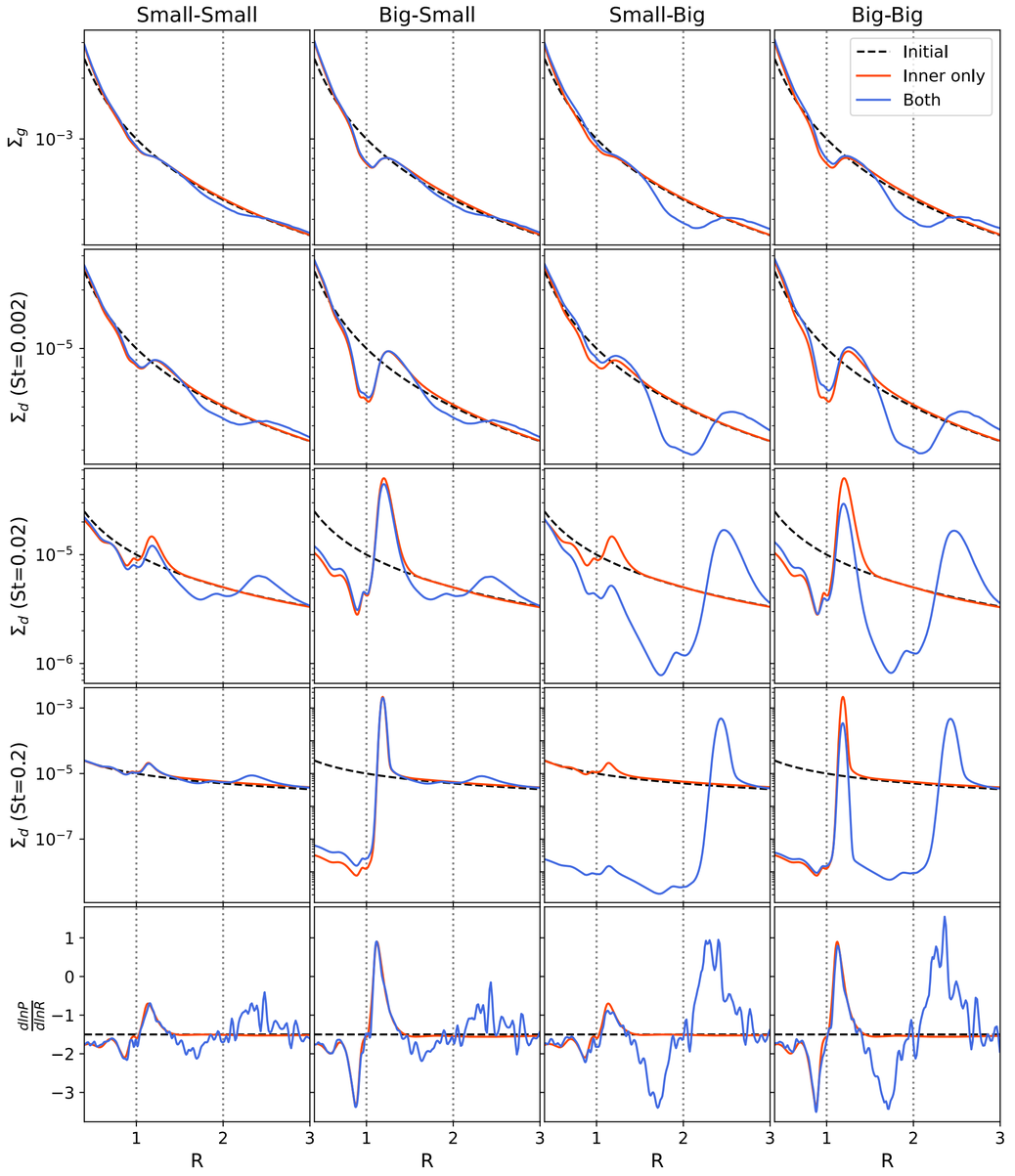

Figure 2. Azimuthally averaged profiles of the four simulations presented in Table 1 with two planets that cause two points of inflections (Small-Small; left), an inner pressure maximum and an outer point of inflection (Big-Small; second column), an inner point of inflection and an outer pressure maximum (Small-Big; third column) and two pressure maxima (Big-Big; right). The location of the two planets are represented by the vertical dotted lines. The simulations with only a single planet (located at R = 1) are shown in a red line for comparison. From top to bottom we present the gas surface density, the dust surface density for St = 0.002, St = 0.02 and St = 0.2 and finally the pressure gradient through the quantity $d\ln P/d\ln R$, all in code units. In cases with a small outer planet (columns 1 and 2) little difference is seen in the interplanetary density profiles (rows 1-4) between the one- and two-planet cases, whereas the difference is substantial for a large outer planet. In particular, for the case where there are two planets present that are massive enough to create two pressure maxima (right column) the amount of dust in the pressure maximum in between the two planets is reduced.

Big-Bigの場合

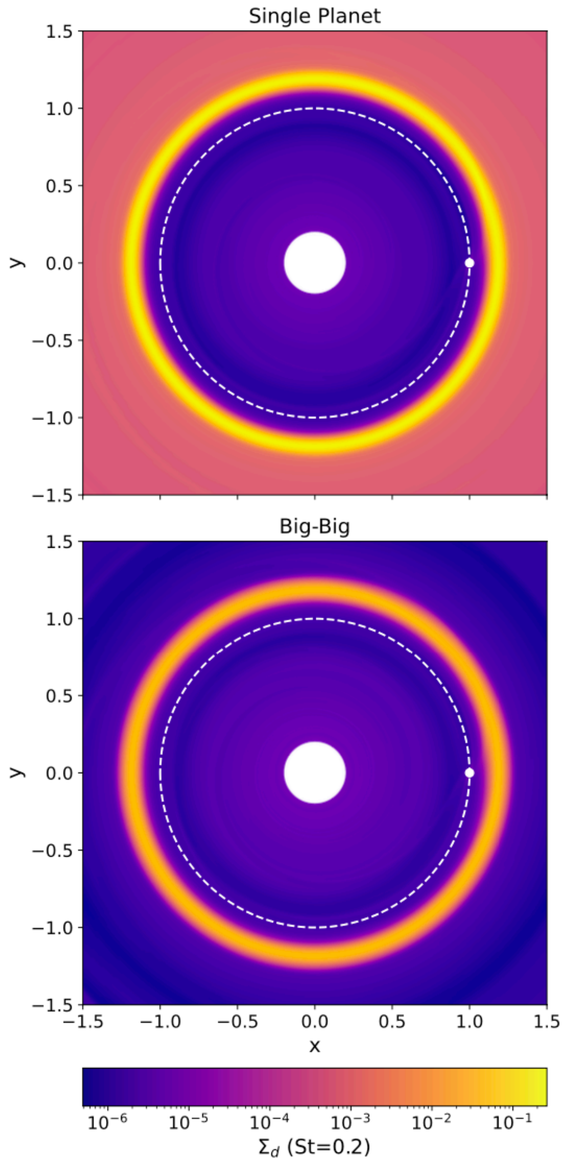

Figure 3. 2D plot of the St = 0.2 dust density for the single $20M_\oplus$ and the two-planet $20M_\oplus$&$35M_\oplus$ (i.e. Big-Big) simulations showing only the inner part of the discs simulated. The inner planet's position is indicated with a white circle, its orbit by the white dotted line. The high density ring exterior to the inner planet's orbit is a potential location for planet formation. In the two-planet case the density in this ring is notably reduced, limiting the mass of any compact bodies that may form here.

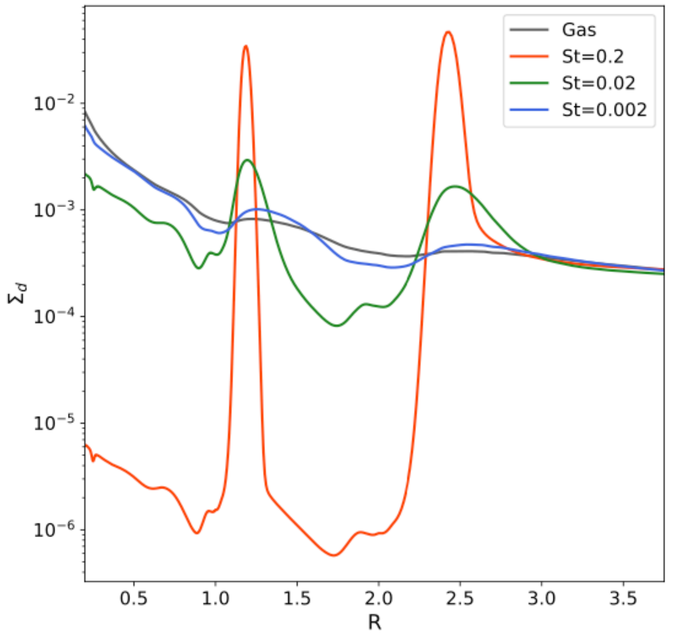

Figure 6. Azimuthally averaged dust surface density profiles for the three simulated dust species and compared to the gas surface density (where the dust is rescaled by our assumed dust-to-gas ratio of 0.01), for the $20M_\oplus$ and $35M_\oplus$ (Big-Big) system. The small dust tends to mostly follow the gas, whilst the larger dust experiences radial drift and dust trapping, resulting in large scale dust depletion in the interplanetary region and the inner disc.

観測例

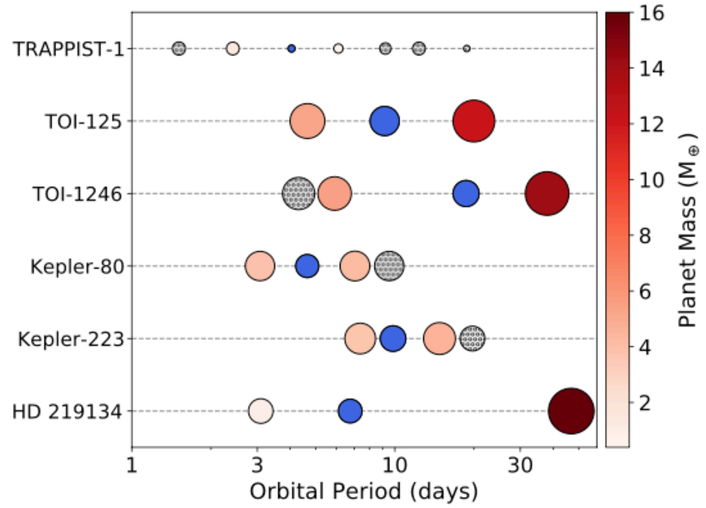

Figure 5. The 6 planetary systems which contain a small planet sandwiched in between two larger planets. The sandwiched planet is highlighted with a blue marker. The size represents the planet's mass as does the colour of the planet either side of the sandwiched planet. The black hatched markers are the other planets in the system.

青色が大きな惑星の間に
ある小さな惑星

47. **Protoplanetary and debris disks in the η Chamaeleontis Association: A sub-millimeter survey obtained with APEX/LABOCA**

V. Roccatagliata, A. Sicilia-Aguilar, M. Kim, J. Campbell-White, M. Fang, S. J. Murphy, S. Wolf, W. A. Lawson, Th. Henning, J. Bouwman

★ Nearby associations are ideal regions to study coeval samples of protoplanetary and debris disks down to late M-type stars. Those aged 5-10,Myrs, where most of the disk should have already dissipated forming planets, are of particular interest. We present the first complete study of both protoplanetary and debris disks in a young region, using the η Chamaeleontis association as a test bench to study the cold disk content. We obtained sub-millimeter data for the entire core population down to late M-type stars, plus a few halo members. We performed a continuum sub-millimeter survey with APEX/LABOCA of all the core populations of η Cha association. Disk properties have been derived by modeling protoplanetary and debris disks using RADMC 2D and DMS, respectively. We find that protoplanetary disks in η Cha typically have holes with radii of the order of 0.01 to 0.03 AU, while ring-like emission from the debris disks is located between 20 au and 650 au from the central star. The parallaxes and Gaia eDR3 photometry, in combination with the PARSEC and COLIBRI isochrones, enable us to confirm an age of η Cha between 7 and 9 Myrs. In general, the disk mass seems insufficient to support accretion over a long time, even for the lowest mass accretors, a clear difference compared with other regions and also a sign that the mass budget is further underestimated. We do not find a correlation between the stellar masses, accretion rates, and disk masses, although this could be due to sample issues. We confirm that the presence of inner holes is not enough to stop accretion unless accompanied by dramatic changes to the total disk mass content. Comparing η Cha with other regions at different ages, we find that the physical processes responsible for debris disks (e.g., dust growth, dust trapping) efficiently act in less than 5 Myrs.

- Hカメレオン星団の中の原始惑星系円盤とデブリ円盤をサブミリ波でサーベイした。
- サブミリ波の観測と，これまでの観測結果をあわせて，円盤のスペクトルをモデルフィットして，円盤の物理量を見積もった。
- Gaiaのデータと星進化理論から星団の年齢（7-9My）を見積もった。

新しい観測：870μmのサブミリ波

その観測結果と，これまでの観測結果をあわせて，スペクトルのモデルフィッティングを行った。

星＋原始惑星系円盤

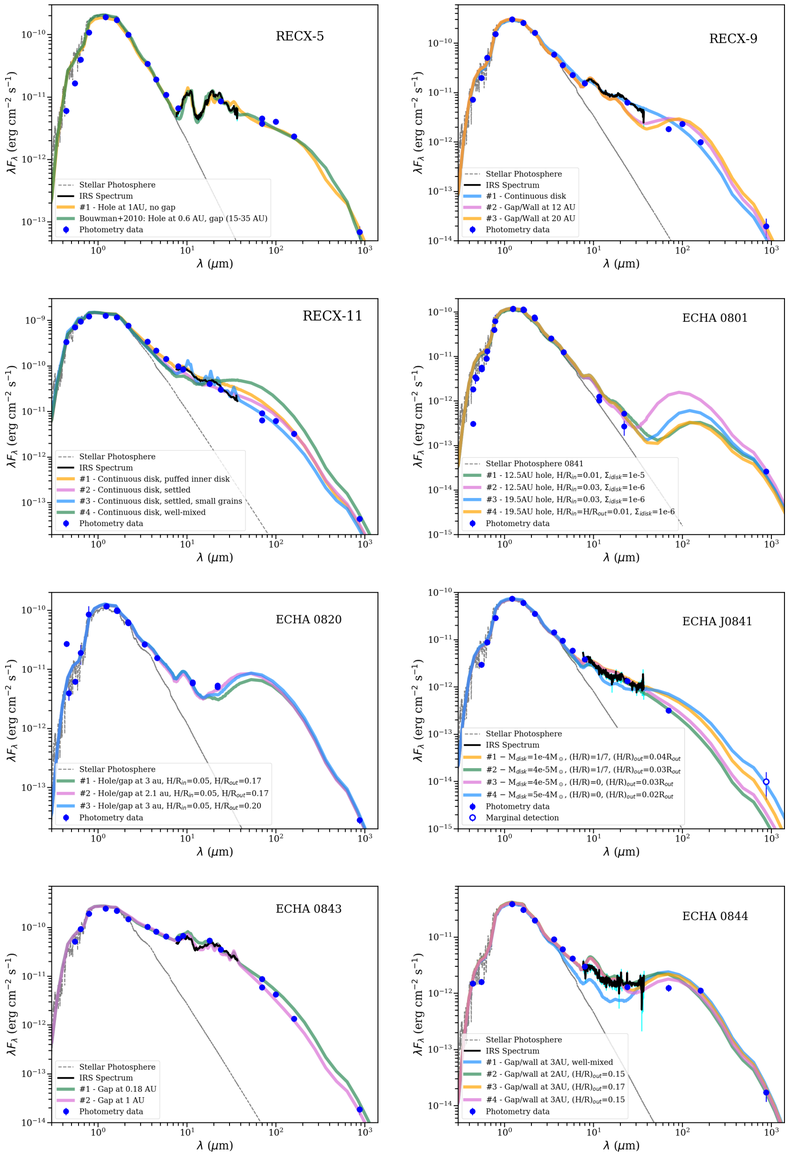

Fig. 2. SED models for the protoplanetary disks. For all cases, the photometry data is marked by blue circles (empty symbols for marginal detections). Spitzer/IRS spectra are plotted in black. The MARCS model stellar photospheres are marked by dotted grey lines, and the various disk models are represented by colored lines and labeled according to their main characteristics (see Table 2). RECX-5: A large-scale gap is not needed to reproduce the long wavelengths, which also means that SED alone cannot constrain among many diverse but equally plausible SED structures. RECX-9: A change in vertical scale height at 10-15 au is needed, which could be caused by a gap, wall, warp, or any other structure affecting the density and the scale height probably created by the existing companion at 20 au. RECX-11: Best fit with relatively massive and flattened disks. A more puffed innermost disk (either a puffed-up rim or a more extended ~0.6 au region) is required, with the disk becoming increasingly flattened and settled at larger radii. J0801 and J0820 appear to be examples of relatively massive transition disks with large, strongly mass-depleted inner holes. ECHA J0841: Very flattened SED. ECHA J0843: Small gap or hole required. For ECHA J0844: Gap and/or change in the vertical scale height needed to explain the far-IR flux.

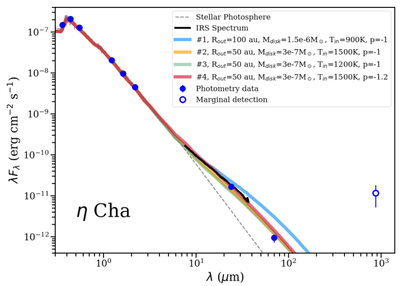

Fig. 3. SED fit for η Cha. Note that the LABOCA 870 μm point is not fitted, as it is most likely contaminated as explained in the text.

星＋デブリ円盤

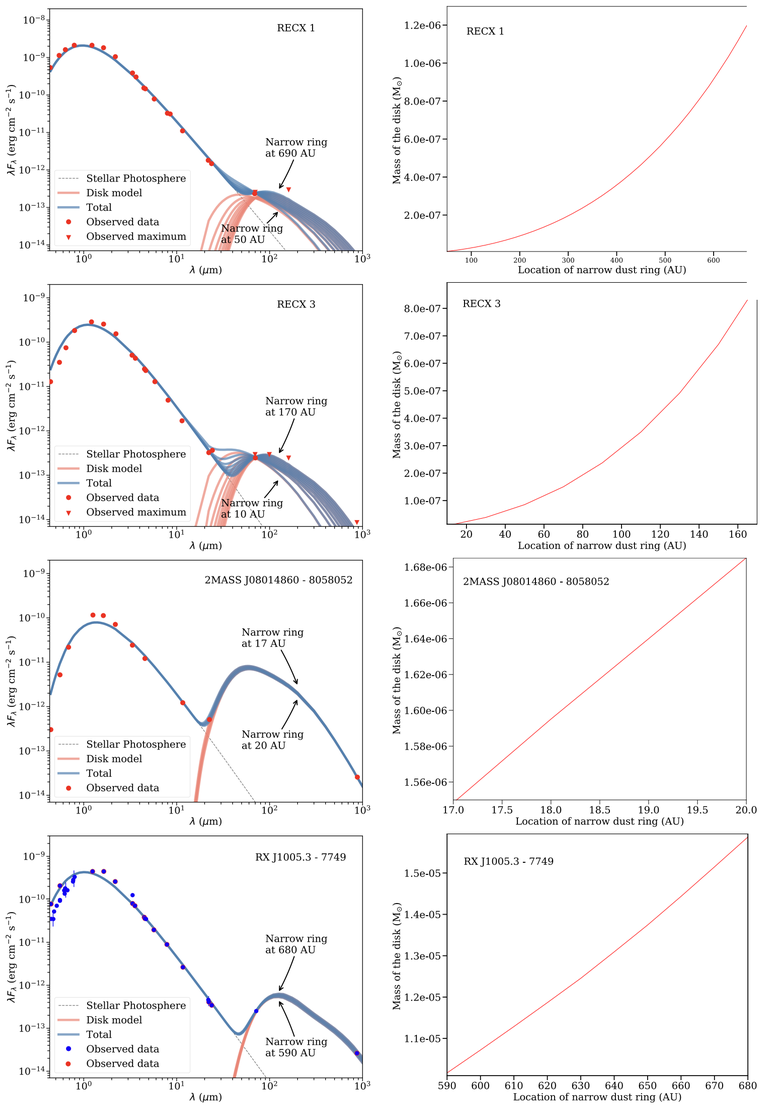

Fig. 4. *Left:* SED models for the debris disks. The photometry data are marked by red circles and triangles (the upper limits). Stellar photospheric, disk, and total emission (stellar photospheric + disk models) are represented by grey dotted lines, and red and blue continuous lines, respectively (see Table 2 for details on individual models). The blue dots in the SED of RX J1005.3-7749 show the detection from Murphy et al. (2010). *Right:* Results of the SED modeling of the debris disks showing the mass of the disk as a function of the location of the narrow dust ring.

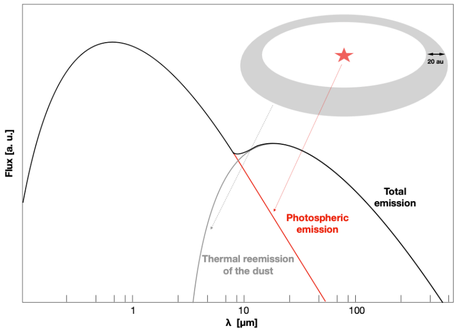

Fig. A.1. Sketch of the basic idea of the model used to interpret the SED of the debris disks.

星団の年齢推定

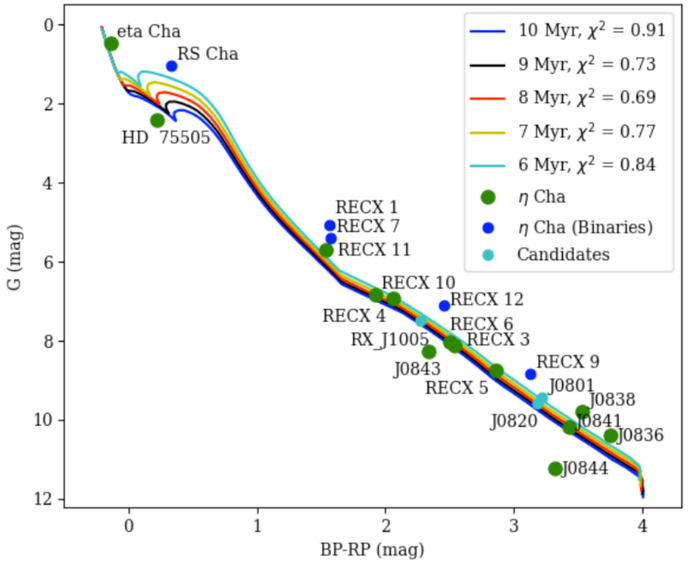

星のスペクトル型と降着率

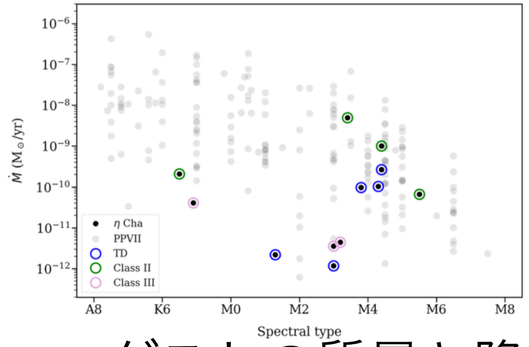

ダストの質量と降着率

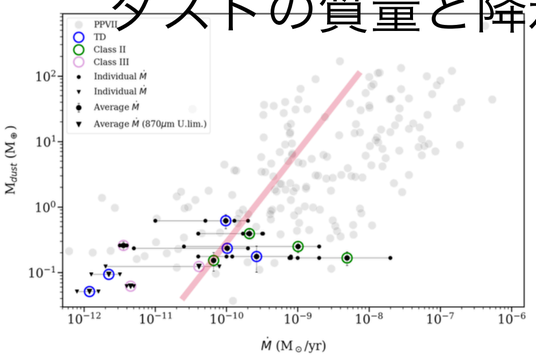

Fig. 6. *Top*: Accretion rate vs spectral type. Note the lack of significant correlations between these quantities. *Bottom*: Circumstellar dust mass derived according to Eqn. 1 vs. accretion rate. For comparison, the objects in the list from Manara et al. (2023) are shown in grey. Note that the total disk mass would depend on the gas-to-dust ratio. APEX flux and mass upper limits are marked by inverted triangles. The red line corresponds to the model fitted by Manara et al. (2016). The accretion rates are taken from the literature (see Table A.1). For each object, we show the individual measurements (small symbols) together with the average rate (large symbols). A further color ring is added to specify the type of disk according to the classical SED classification.

特に相関はなかった

with an optically thin dust emission. With the same approximation as in the other debris systems, we find that ECHA J0841 is the only source with a massive narrow ring of 1.6-1.7 $\times 10^{-6} M_{\odot}$ at between 17 and 20 au from the central star.

It is very interesting to highlight that both approaches led to a large gap of about 15 au and a very massive disk compared to